Separating Fluorescent and Reflective Components by Using a Single Hyperspectral Image

Yinqiang Zheng
National Institute of Informatics
yqzheng@nii.ac.jp

Ying Fu
The University of Tokyo
fuying@iis.u-tokyo.ac.jp

Antony Lam
Saitama University
antonylam@cv.ics.saitama-u.ac.jp

Imari Sato
National Institute of Informatics
imarik@nii.ac.jp

Yoichi Sato
The University of Tokyo
ysato@iis.u-tokyo.ac.jp

Abstract

This paper introduces a novel method to separate fluorescent and reflective components in the spectral domain. In contrast to existing methods, which require to capture two or more images under varying illuminations, we aim to achieve this separation task by using a single hyperspectral image. After identifying the critical hurdle in single-image component separation, we mathematically design the optimal illumination spectrum, which is shown to contain substantial high-frequency components in the frequency domain. This observation, in turn, leads us to recognize a key difference between reflectance and fluorescence in response to the frequency modulation effect of illumination, which fundamentally explains the feasibility of our method. On the practical side, we successfully find an off-the-shelf lamp as the light source, which is strong in irradiance intensity and cheap in cost. A fast linear separation algorithm is developed as well. Experiments using both synthetic data and real images have confirmed the validity of the selected illuminant and the accuracy of our separation algorithm.

1. Introduction

Hyperspectral information has proven to be useful in such applications as high-quality color reproduction, spectra-based material identification, computer-aided medical diagnostics and so on. A great variety of hyperspectral imaging methods and apparatuses (see [3, 11, 14, 19] and many others) have been developed and implemented to capture spectral reflectance of scenes.

Fluorescence is a common optical phenomenon present in many natural objects, like coral, living organic tissues and minerals. Fluorescent substances have also been widely applied to paper and cloth for color augmentation, to cur-

(a) Input   (b) Reflectance   (c) Fluorescence
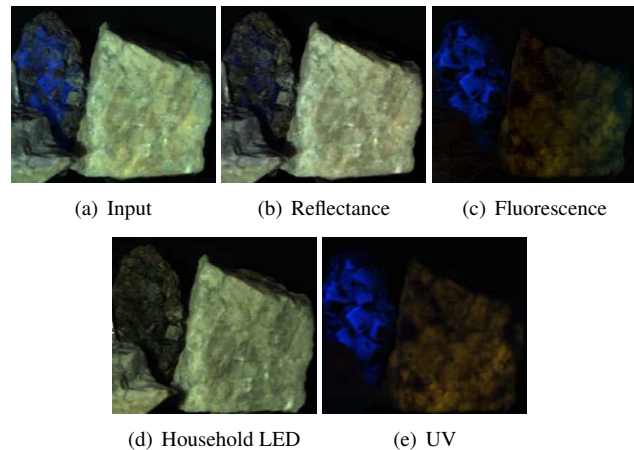
(d) Household LED   (e) UV

Figure 1. Given a single hyperspectral image of some rocks (a) under the selected illuminant, our proposed algorithm can separate the fluorescent component (c) from the reflective one (b). As reference, (d) shows the same scene under a household LED lamp, while (e) shows the scene under a UV light. Since the fluorescent component in these rocks can only be excited under UV irradiance, (d) almost contains the reflective component only.

rency notes for anti-counterfeiting, as well as to biochemical dyes for molecular labeling and tracking.

When the scene contains fluorescence, existing hyperspectral reflectance estimation methods, like those in [11, 19], can not provide accurate estimation. This is because of the well-known wavelength shifting effect of fluorescence that, unlike a reflective surface, fluorescent substances would absorb incident irradiance and re-emit it at longer wavelengths. Considering that fluorescent and reflective components interact with the illumination in quite different ways, it is necessary to separate them from image observations [4, 8, 9, 13, 15].

Existing works [6, 8, 15, 22, 23, 26] have addressed this spectra separation problem, all of which require to capture

two or more images of the same scene under varying illuminations. Given a single image, is it possible to separate the fluorescent and reflective components? To explore this problem is not only conceptually interesting but also practically rewarding. For example, it might simplify the image capturing process and eliminate the burden of switching between illuminations.

In this work, we show, for the first time to our knowledge, the separation is feasible when provided a hyperspectral image captured under an illumination with high-frequency components, see Fig.1 for an example of fluorescent rocks. We start our analysis from a purely mathematical viewpoint, by first introducing the standard low-dimensional linear basis expression for the reflectance and fluorescent emission spectra to reduce the number of variables, and then retrieving the optimal illumination spectrum so as to conquer the dependency issue of these two bases. We examine the Fourier magnitude distribution of the retrieved optimal illumination, and find that it contains substantial high-frequency components. This observation inspires us to investigate the underlying reason why high-frequency components are needed for separation, and finally leads us to recognize a key difference between reflectance and fluorescence in response to the frequency modulation effect of illumination. Specifically, the Fourier magnitude distribution of the reflective component will be modulated by the illumination spectrum, while that of the fluorescent component is independent of illumination Fourier magnitude distribution. This property of fluorescence fundamentally explains the feasibility of separation by using a single hyperspectral image. On the practical side, we successfully find an off-the-shelf high-intensity discharge (HID) lamp as the light source, which is strong in irradiance intensity and cheap in cost. A fast linear separation algorithm is developed to handle high resolution images as well. Experiments using both synthetic data and real images have confirmed the validity of the selected illuminant and the accuracy of our separation algorithm.

Our major contributions can be summarized as follows: (i). We numerically design the optimal illumination spectrum to conquer the dependency issue of the fluorescent emission and reflectance bases; (ii). We analytically disclose when and why fluorescence and reflectance separation by using a single hyperspectral image is feasible; (iii). We find an off-the-shelf lamp as the light source and develop an efficient linear separation algorithm.

The remaining parts of this paper are organized as follows. In Sec.2, we give a more detailed literature review. Sec.3 includes the numerical design of illumination spectrum, followed by the theoretical analysis and the linear separation algorithm. We show some experimental results in Sec.4, and conclude this work in Sec.5.

2. Related Works

Due to its special wavelength shifting effect and color constancy, fluorescence has recently received much attention in computer vision, along with various successful applications to shape recovery [12, 21, 24], camera photometric calibration [10] and inter-reflection removal [7].

Fluorescent objects contain both fluorescent and reflective components. Due to the difference in their mechanisms when interacting with the illumination, it is necessary to separate these two components from image observations. This spectra separation task has shown to be critical for color relighting [8, 13, 15], coral reef monitoring [9] and cancer diagnosis in biomedical engineering [4]. In the following, we review the most closely related works on fluorescence and reflectance separation.

Thanks to the color invariance property of fluorescence, researchers in [25] have been able to separate fluorescence from reflectance by using two RGB images under different yet unknown illuminations via independent component analysis. Rather than being satisfied with RGB colors of fluorescence and reflectance, Fu *et al.* [6] have tried to recover their spectra by using as many as nine RGB images captured under varying color illuminations.

In addition to wideband RGB cameras, hyperspectral imaging devices have also been widely used for fluorescence and reflectance spectra separation. For example, the well-known bispectral method [16] coordinates a monochromator and a spectrometer to measure the reflective and fluorescent spectra of a single scene point in an exhaustive manner. Lam and Sato [15] used a hyperspectral image sensor instead, and introduced the linear basis expression of reflectance and fluorescence spectra so as to reduce the required number of measurements, although about twenty images are still needed. The bispectral coding scheme [22] is rooted in the classical bispectral measurement method as well, in which dozens of hyperspectral images have to be captured under shifting narrow-band illuminations.

To further reduce the number of images, Tominaga et al. [23] implicitly assumed that the scene contains no blue fluorescence, and successfully separated these two components by using two hyperspectral images under ordinary illuminants. Fu et al. [8] relaxed this assumption, at least in principle, by using two high-frequency and complementary sinusoid illuminations defined in the spectral domain. The reason of using such specialized illuminations lies in their demanding requirement that the fluorescent absorption scalars under two different illuminations should be the same. The resulting separation algorithm is very simple and its accuracy is outstanding. Unfortunately, the specialized illumination spectra were generated by a programmable light source in [8], which is expensive in cost and weak in irradiance intensity. As a result, one has to reduce the camera frame rate

so as to capture a bright enough image. Zheng et al. [26] introduced one more hyperspectral image, and were able to use ordinary illuminants instead, but at the added cost of solving a more complicated bilinear problem via iterations.

To use multiple images under varying illuminations complicates the data capturing process (*e.g.* synchronization operation of the camera and illumination). This motivates us to explore the possibility of using a single hyperspectral image for this separation task. In the following, we are going to examine requirements of the illumination spectrum, look for an off-the-shelf lamp as the illuminant and develop a fast linear algorithm for separation.

3. Fluorescence and Reflectance Separation of a Hyperspectral Image

3.1. Hyperspectral Fluorescence Imaging Model

For a pure reflective surface, the radiance $i_1(\lambda)$ at wavelength λ is a direct product of the irradiance $l(\lambda)$ and the reflectance coefficient $r(\lambda)$, i.e., $i_1(\lambda) = l(\lambda)r(\lambda)$.

In contrast, a pure fluorescent surface would first absorb some energy in shorter wavelengths and re-emit it in longer wavelengths. According to [8, 25], this shifting effect can be approximately described by $i_2(\lambda) = \left(\int l(\tilde{\lambda})a(\tilde{\lambda})d\tilde{\lambda} \right) e(\lambda)$, in which $a(\lambda)$ and $e(\lambda)$ denote the absorption and emission intensity at λ, respectively.

Let us recall that a usual fluorescent object contains both the reflective and fluorescent components. Therefore, the hyperspectral imaging equation of a fluorescent-reflective surface reads

$$i(\lambda) = i_1(\lambda) + i_2(\lambda) = l(\lambda)r(\lambda) + \left(\int l(\tilde{\lambda})a(\tilde{\lambda})d\tilde{\lambda} \right) e(\lambda). \quad (1)$$

Given a proper illumination spectrum $\mathbf{l} = \left[l_{\lambda_1}, l_{\lambda_2}, \cdots, l_{\lambda_n} \right]^T$ and its corresponding radiance of a scene point $\mathbf{i} = \left[i_{\lambda_1}, i_{\lambda_2}, \cdots, i_{\lambda_n} \right]^T$ recorded by a hypersepctral device with n bands, the imaging equation in Eqn.1 can be rewritten as

$$\mathbf{i} = L\mathbf{r} + \left(\int l(\tilde{\lambda})a(\tilde{\lambda})d\tilde{\lambda} \right)\mathbf{e} = L\mathbf{r} + s\mathbf{e} = L\mathbf{r} + \hat{\mathbf{e}}, \quad (2)$$

where $L = diag(l_{\lambda_1}, l_{\lambda_2}, \cdots, l_{\lambda_n})$, and $\mathbf{r} = \left[r_{\lambda_1}, r_{\lambda_2}, \cdots, r_{\lambda_n} \right]^T$ denotes the reflectance spectrum. $\mathbf{e} = \left[e_{\lambda_1}, e_{\lambda_2}, \cdots, e_{\lambda_n} \right]^T$ represents the fluorescent emission spectrum. We have assumed that the response function of the hyperspectral device has been normalized.

Note that the absorption spectrum $\mathbf{a} = \left[a_{\lambda_1}, a_{\lambda_2}, \cdots, a_{\lambda_n} \right]^T$ is also important in describing the spectral behavior of fluorescence. From Eqn.2, we see that it simply integrates with the light source to a scalar $s = \int l(\tilde{\lambda})a(\tilde{\lambda})d\tilde{\lambda}$ that scales the emission spectrum $\mathbf{e}$. Due

to a scale ambiguity between s and $\mathbf{e}$, we can without loss of generality merge them into $\hat{\mathbf{e}}$. Our objective is to separate a hyperspectral measurement $\mathbf{i}$ into the reflectance part $\mathbf{r}$ and the fluorescent part $\hat{\mathbf{e}}$, by using a proper illumination spectrum $\mathbf{l}$.

The number of constraints in Eqn.2 is n, thus we can not directly determine $2n$ variables in $\mathbf{r}$ and $\hat{\mathbf{e}}$. A straightforward idea to resolve this issue is to introduce some low-dimensional models so as to reduce the number of variables. Both linear and nonlinear low-dimensional models have been suggested for reflectance [17, 20] and fluorescent emission spectra [15, 26]. Due to its simplicity, we choose the linear low-dimensional expression. By embedding linear basis models into Eqn.2, we obtain

$$\mathbf{i} = L\mathbf{r} + \hat{\mathbf{e}} = LA\boldsymbol{\alpha} + B\boldsymbol{\beta} = \begin{bmatrix} LA & B \end{bmatrix} \begin{bmatrix} \boldsymbol{\alpha}^T & \boldsymbol{\beta}^T \end{bmatrix}^T, \quad (3)$$

where $A^{n \times u}$ and $\boldsymbol{\alpha}^{u \times 1}$ are the reflectance bases and coefficients, while $B^{n \times v}$ and $\boldsymbol{\beta}^{v \times 1}$ the bases and coefficients for fluorescent emission. u and v denote the number of bases for reflectance and fluorescent emission, respectively. We can use the principle component analysis (PCA) of the training data to determine data-dependent bases A and B[1]. According to [15, 17, 20], the number of reflectance bases u is usually 8, while that of fluorescent emission bases v is about 12.

At first glance, Eqn.3 seems to be well-posed, since the number of constraints n is usually much greater than the total number of bases $(8 + 12 = 20)$. Unfortunately, as recognized in [26], the bases A and B from PCA training are not completely independent. In other words, when the illumination is spectrally white, the matrix $\begin{bmatrix} LA & B \end{bmatrix}$ degenerates to $\begin{bmatrix} A & B \end{bmatrix}$, whose condition number approaches infinity. Under this condition, the coefficients $\begin{bmatrix} \boldsymbol{\alpha}^T & \boldsymbol{\beta}^T \end{bmatrix}^T$ can not be uniquely determined, and the separation task is therefore infeasible. In the following, to resolve the challenging basis dependency issue, we first mathematically design the illumination spectra by minimizing a condition number criterion.

3.2. Numerically Optimal Illumination Spectrum

Here, we borrow the concept in linear algebra that a linear equation becomes more robust as the condition number of the coefficient matrix reduces. Given the bases A and B, we try to find an optimal illumination spectrum $\mathbf{l}^*$ such that the condition number of $\begin{bmatrix} LA & B \end{bmatrix}$ is minimized, that is, $\mathbf{l}^* = argmin_{\mathbf{l}} \; cond\left(\begin{bmatrix} LA & B \end{bmatrix} \right)$. Hereafter, we denote $\begin{bmatrix} LA & B \end{bmatrix}$ as $M(\mathbf{l})$ for brevity.

---

[1]In all our experiments, we use PCA on the Munsell reflectance spectra dataset [20] to obtain the reflectance bases A, while the McNamara fluorescent spectra dataset [18] to train the fluorescent emission bases B.

(a) OPTIMAL (1.8) (b) ELS (4.9) (c) D2C (12.4) (d) OFFICE (55.2) (e) COLOR LEDs(74.0) (f) WHITE LED (301.5)

(g) Fourier Magnitude Distribution of Illumination Spectra from (a) to (f)

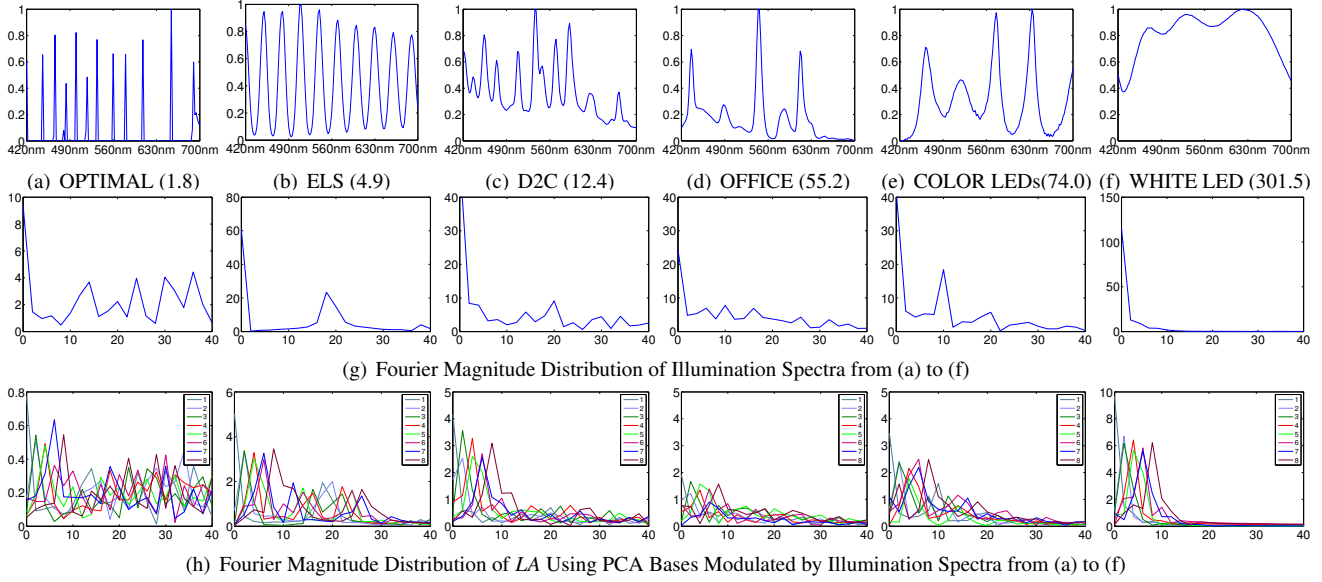(h) Fourier Magnitude Distribution of LA Using PCA Bases Modulated by Illumination Spectra from (a) to (f)

Figure 2. Various illumination spectra and their Fourier magnitude distribution. The first row shows the retrieved optimal illumination spectrum (a), the spiky spectrum generated by ELS (b), the spectrum of the D2C lamp (c), the office fluorescent lamp spectrum (d), the composite spectrum from five color LEDs (e) and the spectrum of a 5000K white LED lamp (f). Their corresponding condition number of $M(\mathbf{l})$ is shown in the parentheses. The Fourier magnitude distributions of these six illumination spectra are shown in (g), while those of LA are shown in (h).

To minimize the condition number of a linearly parameterized rectangular matrix is very challenging, since the objective function is not differentiable, which would frustrate most derivative-based minimization algorithms. In the following, we transform it into a bilinear matrix inequality (BMI) optimization problem. BMI has been extensively explored in control theory [1], for which there exist some complimentary off-the-shelf softwares, such as PENLAB [5].

Considering that a univariate quadratic function $f(z) = z^2, z \geq 0$, is monotonically increasing, we minimize the following equivalent problem instead

$$\min_{\mathbf{l}} \ cond^2\left(M(\mathbf{l})\right) = cond\left(M(\mathbf{l})^T M(\mathbf{l})\right). \quad (4)$$

According to [2], in order to minimize the condition number of the parametric positive definite matrix, Eqn. (4) can be rewritten into a fractional matrix inequality problem

$$\min_{x,y,\mathbf{l}} \ x, \ s.t., \ I_1 \leq y^{-1} M(\mathbf{l})^T M(\mathbf{l}) \leq xI_1, y > 0, \quad (5)$$

in which I_1 is the $(u+v)$-dimensional identity matrix.

Thanks to the Schur complement lemma, the following equivalence holds

$$\frac{1}{y} M(\mathbf{l})^T M(\mathbf{l}) \leq xI_1, y > 0 \Leftrightarrow \begin{bmatrix} xI_1 & M(\mathbf{l})^T \\ M(\mathbf{l}) & yI_2 \end{bmatrix} \succeq \mathbf{0}, \quad (6)$$

where I_2 is the n-dimensional identity matrix.

Therefore, the condition number minimization problem in Eqn.4 can be reformulated into the following bilinear ma-trix inequality problem

$$\min_{x,y,\mathbf{l}} \ x, \ s.t., \ \begin{bmatrix} xI_1 & M(\mathbf{l})^T \\ M(\mathbf{l}) & yI_2 \end{bmatrix} \succeq \mathbf{0}, M(\mathbf{l})^T M(\mathbf{l}) \succeq yI_1, y > 0. \quad (7)$$

The bilinearity arises from the multiplication of $M(\mathbf{l})^T$ and $M(\mathbf{l})$, which is the only nonconvex constraint in Eqn.7. This problem can be directly solved by using the PENLAB software [5].

Using the 8-D PCA reflectance bases for A and 12-D PCA fluorescence bases for B, PENLAB returns the retrieved optimal illumination spectrum in the 420nm-700nm range, as shown in Fig.2(a). The corresponding condition number of $M(\mathbf{l})$ is 1.8. Note that, we have run PENLAB 5000 times by starting from random initialization, and this reported condition number is the smallest one. In this sense, we call the retrieved spectrum as the optimal spectrum. From Fig.2(a), we see that the optimal spectrum is very spiky, and contains substantial high-frequency components, as revealed by its Fourier magnitude distribution in the first subfigure of Fig.2(g).

3.3. Frequency Domain Analysis

Why are high-frequency components needed for our separation task? By considering the imaging equation in Eqn.3, we have come up with an explanation from the viewpoint of frequency modulation. Specifically, we can interpret the illumination spectrum $\mathbf{l}$ as a modulating signal of the reflectance bases A, whose spectral distribution has no effect at all on the fluorescent emission bases B, because of the

(a) D2C (b) Ballast and Igniter (c) Nikon ELS

Figure 3. The 6000K D2C HID lamp (a) and its driving accessories (b). The input voltage is 12V and the power is 55W. The whole set costs about 30 USD, which is much more economical than the programmable ELS (c).

integration in Eqn.1. The condition number minimization operation in Eqn.4 is to find a proper modulating signal such that the correlation between *LA* and *B* is as small as possible. When **l** contains high-frequency components, the frequency of *A* can be lifted significantly, and thus the overlap of *LA* and *B* in the frequency-domain is greatly reduced. This point can be easily observed by comparing the Fourier magnitude distribution of *LA* in the first and last subfigure of Fig.2(h).

We have further analyzed the requirements on the illumination spectrum by means of frequency-domain signal processing. This theoretical analysis is presented in the supplementary material, since it is quite lengthy.

3.4. Illumination Spectra in Practice

When a programmable light source is available, we can generate an illumination spectrum that approximates the numerically optimal spectrum very well. For example, by using a Nikon Equalized Lighting Source (ELS), we are able to generate a spiky illumination spectrum with a condition number of 4.9, as shown in Fig.2(b).

However, the irradiance intensity of this programmable light source is quite weak, and as a consequence, the camera has to be slowed down so as to capture a bright enough image. This forces us to find a very strong lamp as the light source.

We have examined the spectra of tens of ordinary lamps in daily life. Among them, we recognize that the D2C (6000K) HID lamp (see Fig.3) has very strong irradiance due to its special lighting mechanism, and its spectrum is highly spiky as shown in Fig.2(c). Its corresponding condition number is 12.4. This lamp is cheap and easily available, since it is widely used as headlights in many brands of cars. The office fluorescent lamp has a spiky spectrum as well, as shown in Fig.2(d). Unfortunately, it has three spikes only, and the resulting condition number is 55.2.

We have also tried to generate a spiky illumination spectrum by combining five narrow-band color LEDs, as shown in Fig.2(e). It leads to a condition number of 74.0. We believe that the primary reason lies in that the bandwidth of the LEDs that we have is not narrow enough.

As comparison, we show the smooth spectrum of a

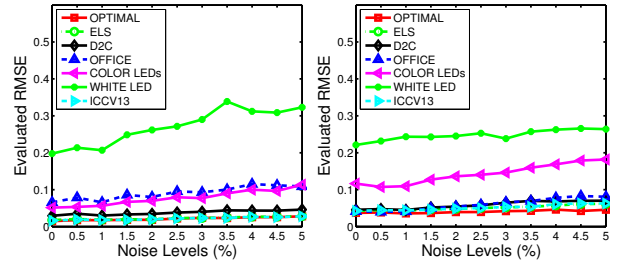
(a) Reflectance (b) Fluorescent Emission

Figure 4. Experiment results using synthetic data on the noise sensitivity of our proposed method under the *OPTIMAL*, *ELS*, *D2C*, *OFFICE*, *COLOR LEDs* and *WHITE LED* illuminations shown in Fig.2(a-f), as well as that of the *ICCV13* method.

5000K white LED lamp in Fig.2(f), whose corresponding condition number is 301.5.

We present the Fourier magnitude distribution of these six illumination spectra in Fig.2(g). We can observe that, similar to the optimal spectrum, both the spiky spectrum by ELS and the D2C spectrum contain a large amount of high-frequency components, which substantially lift the frequency of *A*, as shown in Fig.2(h). As expected, the white LED spectrum has almost no high-frequency components, and is inappropriate for the spectra separation task.

3.5. Separation Algorithm

After the illumination spectrum **l** is determined, on the basis of Eqn.3, we can easily separate the fluorescent and reflective components by $\begin{bmatrix} \boldsymbol{\alpha}^T & \boldsymbol{\beta}^T \end{bmatrix}^T = \begin{bmatrix} LA & B \end{bmatrix}^+ \mathbf{i} = M^+\mathbf{i}$, in which M^+ denotes the Moore-Penrose pseudoinverse of $M = \begin{bmatrix} LA & B \end{bmatrix}$.

When capturing a whole scene by using a hyperspectral camera, we can separate all pixels simultaneously under the assumption that the illumination is uniform across the scene by using the following linear operation

$$\begin{bmatrix} \boldsymbol{\alpha}_1 & \boldsymbol{\alpha}_2 & \cdots & \boldsymbol{\alpha}_m \\ \boldsymbol{\beta}_1 & \boldsymbol{\beta}_2 & \cdots & \boldsymbol{\beta}_m \end{bmatrix} = M^+ \begin{bmatrix} \mathbf{i}_1 & \mathbf{i}_2 & \cdots & \mathbf{i}_m \end{bmatrix}, \quad (8)$$

where *m* is the total number of pixels. Note that *m* can be very large for a high-resolution hyperspectral image, however, this causes little difficulty, due to the fact that M^+ can be precomputed offline and one only needs to multiply M^+ with the image measurement matrix $\begin{bmatrix} \mathbf{i}_1 & \mathbf{i}_2 & \cdots & \mathbf{i}_m \end{bmatrix}$. As for the running time, our algorithm takes about 40 milliseconds in MATLAB (2012a) on a desktop with a 4-core i7-3770 CPU (3.4GHz) and 8GB memory, for a hyperspectral cube with 57 bands and 640×512 spatial resolution.

3.6. Comparison with the State-of-the-Art [8]

As mentioned in Sec.2, the method in [8] also uses high-frequency illuminations. Therefore, it would be interesting to disclose the difference between our method and [8] in

more detail. The fundamental requirement in [8] is that the absorption scalars under two different illuminations should be the same. Specifically, given two illuminations $\mathbf{l}_1$ and $\mathbf{l}_2$, we can obtain two equations on the basis of Eqn.2 as follows

$$
\begin{aligned}
\mathbf{i}_1 &= L_1\mathbf{r} + \left(\int l_1(\tilde{\lambda})a(\tilde{\lambda})d\tilde{\lambda}\right)\mathbf{e} = L_1\mathbf{r} + s_1\mathbf{e}, \\
\mathbf{i}_2 &= L_2\mathbf{r} + \left(\int l_2(\tilde{\lambda})a(\tilde{\lambda})d\tilde{\lambda}\right)\mathbf{e} = L_2\mathbf{r} + s_2\mathbf{e}.
\end{aligned}
\tag{9}
$$

To make sure that s_1 equals s_2, a natural choice is to use two high-frequency and complementary illumination spectra. What makes the illuminations difficult to generate is the complementary restriction over the whole working spectral range, although a spectrum with high-frequency components is not uncommon. This might be the reason why [8] used a less widely available programmable lighting source as the illuminant.

In contrast, our method relies on the difference in fluorescent and reflective components, when responding to the frequency modulation effect of illumination. The specific spectrum shape does not matter that much, as long as it contains sufficient high-frequency components. This point allows us to find an off-the-shelf lamp as the illuminant, as shown in Sec.3.4.

4. Experiments

4.1. Synthetic Data

We first evaluate the accuracy of our proposed method under various illumination spectra by using synthetic data, and show how it compares with that of the state-of-the-art method [8] using two high-frequency and complementary sinusoid illuminations (referred to as *ICCV13*). For our separation algorithm, we evaluate all the six illumination spectra shown in Fig.2(a-f).

At each independent trial, we randomly select one spectrum from the 18 color patches on the Macbeth color checker as reflectance, and randomly choose one fluorescent absorption-emission spectra pair from the fluorescent spectra dataset [18]. To simulate image disturbance, Gaussian noise is added onto the synthesized hyperspectral signals, whose standard deviations vary from 0 to 5% relative magnitude. At each noise level, we calculate the root mean square error (RMSE) between the estimated spectra and their corresponding ground truth. According to the analysis in [8], we set the period of the high-frequency sinusoid illuminations to be 40 nm.

Fig.4(a) and Fig.4(b) show the average RMSE over 100 independent trials for reflectance and fluorescent emission. As expected, the theoretically optimal spectrum (*OPTIMAL*) makes the separation quite accurate and robust to image noise. Although the *ELS* spectrum has almost the
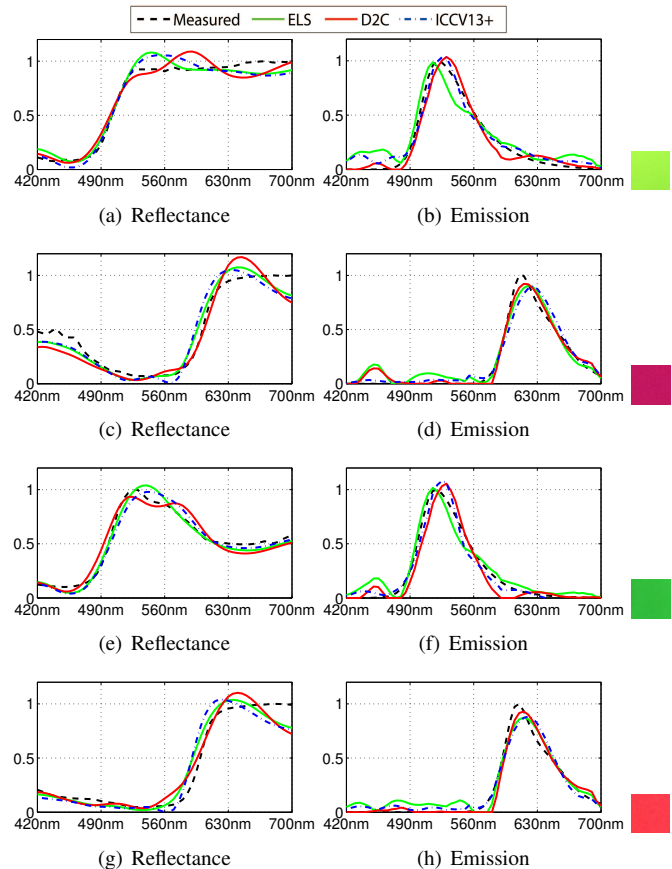

Figure 5. Comparison of the estimated spectra of four color fluorescent patches from our method under the *D2C* and *ELS* illuminations, as well as those from the *ICCV13* method.

same effect as *OPTIMAL*, its real applications are still limited, due to the weak irradiance intensity of the programming light source. The separation accuracy of our selected *D2C* illumination is sufficiently close to that of *OPTIMAL* and *ELS*. The results from using the office fluorescent lamp spectrum (*OFFICE*), the composite spectrum from multiple color LEDs (*COLOR LEDs*) and the white LED spectrum (*WHITE LED*) are not accurate, since their corresponding condition numbers are large.

4.2. Real Images

We use an EBA Japan NH-7 hyperspectral camera to capture images, whose spatial resolution is 1280×1024 pixels. It has 57 bands from 420nm to 700nm, with an interval of 5nm. We use the Nikon ELS to generate high-frequency sinusoid illumination spectra for the *ICCV13* method, whose period is 40 nm. Note that, since the irradiance intensity of the ELS is weak, the capture speed under our selected D2C lamp is more than 100 times faster than under the ELS.

We first measure the reflectance and fluorescent emission spectra of the four fluorescent patches in the right most col-

(a) Input   (b) Ref (Ours)   (c) Fluo (Ours)   (d) Ref (ICCV13)   (e) Fluo (ICCV13)   (f) UV

(g) Blue   (h) Relighted w/ Fluo   (i) Relighted w/o Fluo   (j) Green   (k) Relighted w/ Fluo   (l) Relighted w/o Fluo
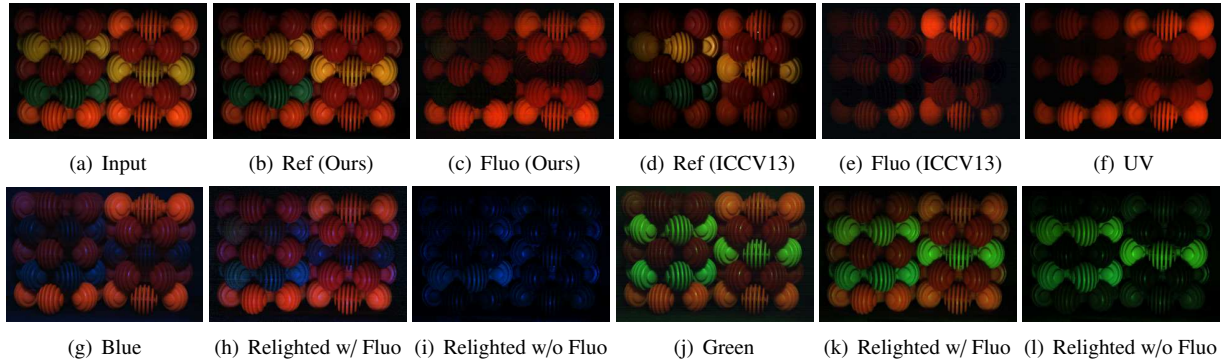
Figure 6. Fluorescence and reflectance spectra separation of the plastic roller scene. From left to right, the first row shows the scene under the D2C illuminant, the separated reflective and fluorescent components from our method and those from the *ICCV13* method using high-frequency sinusoid illuminations. The scene under a UV lamp is shown at the right most for visual comparison. The second row shows the original image and its relighted image with/without fluorescence under blue and green lights.

(a) Input   (b) Ref (Ours)   (c) Fluo (Ours)   (d) Ref (ICCV13)   (e) Fluo (ICCV13)   (f) UV

(g) Blue   (h) Relighted w/ Fluo   (i) Relighted w/o Fluo   (j) Green   (k) Relighted w/ Fluo   (l) Relighted w/o Fluo
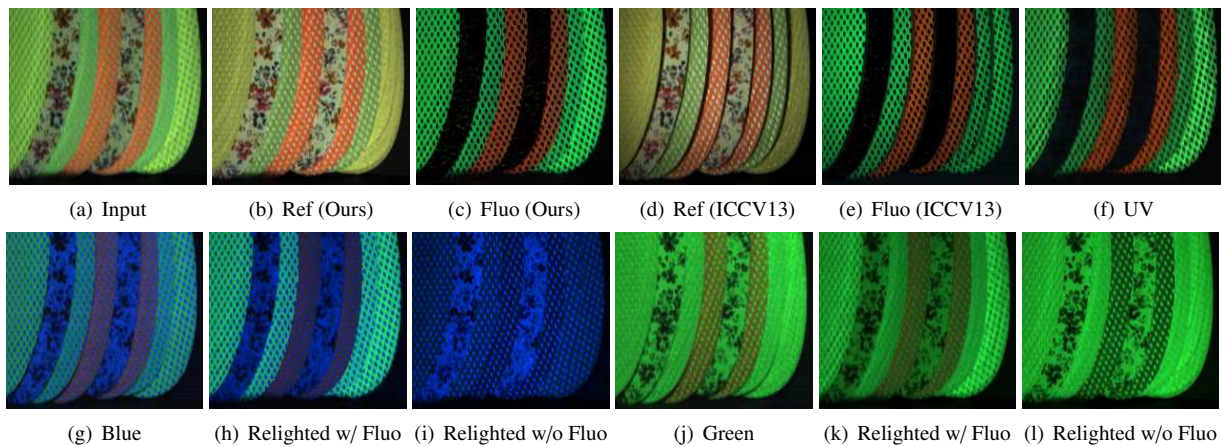
Figure 7. Fluorescence and reflectance spectra separation of the mesh-like pad scene and relighting under novel color illuminations. The subfigures are arranged in the same way as that of Fig.6.

umn of Fig.5, which are used as ground truth. Fig.5 shows the comparison between the ground truth and the estimated spectra from our method under *ELS* and *D2C*, as well as the results from *ICCV13*. From Fig.5, we observe that our method under the ordinary D2C illuminant is comparable to the state-of-the-art method in [8].

We have also used our method under the D2C lamp to separate some other scenes with fluorescence, such as the plastic roller scene in Fig.6 and the mesh-like pad scene in Fig.7. Both our method and the *ICCV13* method achieve satisfactory separation results for these two scenes with strong fluorescence. The cloth scene in Fig.8 contains weak blue fluorescence in the white area. It is a common practice in the printing and painting industry to add some blue fluorescence for whitening. Although the *ICCV13* method itself can handle scenes with blue fluorescence, the used ELS illuminant contains almost no UV irradiance, and the blue fluorescence is thus rarely excited. Our D2C lamp has some irradiance in the UV range, and is able to excite blue fluorescence. This explains why our separated results are better than those of *ICCV13* in Fig.8. We believe that the capabil-

ity of our method to handle scenes with weak fluorescene in the blue range would significantly widen the application scope of hyperspectral fluorescence imaging.

One important application of the separated fluorescence and reflectance spectra is to relight the scene under novel color illuminations. To this end, we further estimate the absorption spectra from the separated fluorescent component $\hat{\mathbf{e}}$ in Eqn.2, by using the sparse dictionary method in [8]. The second row of Fig.6 and Fig.7 shows the captured and relighted scenes under blue and green illuminations. When fluorescence is considered, color discrepancy between the relighted scene and the captured one can be drastically alleviated. This justifies the necessity of taking fluorescence into consideration for fluorescent-reflective scenes.

Our selected strong illuminant and fast separation algorithm pave the way for hyperspectral fluorescence imaging of dynamic scenes. Unfortunately, due to the speed limitation of our current hyperspectral camera, we are not able to capture real-time hyperspectral video. In spite of that, we have tried to demonstrate this potential by slowly moving scene objects, and obtained some preliminary results for an

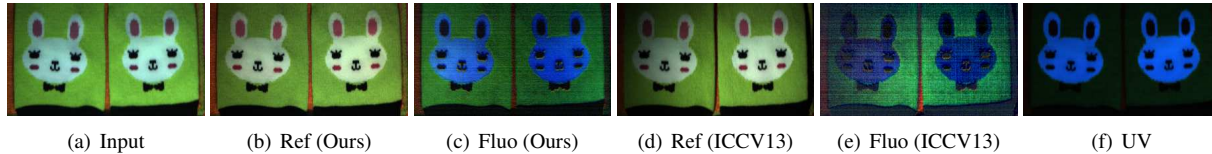| (a) Input | (b) Ref (Ours) | (c) Fluo (Ours) | (d) Ref (ICCV13) | (e) Fluo (ICCV13) | (f) UV |

Figure 8. Fluorescence and reflectance spectra separation of the cloth scene with weak green and blue fluorescence.

image sequence of a tennis ball, which are provided in the supplementary materials.

5. Conclusions and Discussions

We have explored the requirements for illumination spectra so as to enable the challenging task of separating fluorescence and reflectance by using a single hyperspectral image. Guided by our numerically optimal design of the illumination spectrum, we have successfully found an off-the-shelf and high-intensity lamp as the light source. Our proposed separation algorithm is simple to implement and fast enough to handle high-resolution hyperspectral images. Experiments have verified the accuracy of our proposed method.

As shown in Fig.5, the estimated spectra from our method tend to be oversmoothed, or to be slightly oscillating when the original spectral segment is flat. This is a common problem when using linear basis expression for inverse inference with noise. To alleviate this issue by finding an even better illuminant is left as future work.

References

[1] J. V. Antwerp and R. Braatz. A tutorial on linear and bilinear matrix inequalities. *Journal of Process Control*, 10(4):363–385, 2000. 4

[2] S. Boyd and L. Vandenberghe. *Convex Optimization*. Cambridge University Press, 1st edition, 2004. 4

[3] C. Chane, A. Mansouri, F. Marzani, and F. Boochs. Integration of 3D and multispectral data for cultural heritage applications: survey and perspectives. *Image and Vision Computing*, 31(1):91–102, 2013. 1

[4] D. Ferris, R. Lawhead, and E. Dickman. Multimodal hyperspectral imaging for the noninvasive diagnosis of cervical neoplasia. *Journal of Lower Genital Tract Disease*, 5(2):65–72, 2001. 1, 2

[5] J. Fiala, M. Kocvara, and M. Stingl. PENLAB: A MATLAB solver for nonlinear semidefinite optimization. *arXiv preprint arXiv:1311.5240*, pages 1–25, 2013. 4

[6] Y. Fu, A. Lam, Y. Kobashi, I. Sato, T. Okabe, and Y. Sato. Reflectance and fluorescent spectra recovery based on fluorescent chromaticity invariance under varying illumination. *IEEE Conference on Computer Vision and Pattern Recognition*, pages 2163–2170, 2014. 1, 2

[7] Y. Fu, A. Lam, Y. Matsushita, I. Sato, and Y. Sato. Interreflection removal using fluorescence. *European Conference on Computer Vision*, pages 203–217, 2014. 2

[8] Y. Fu, A. Lam, I. Sato, T. Okabe, and Y. Sato. Separating reflective and fluorescent components using high frequency illumination in the spectral domain. *IEEE International Conference on Computer Vision*, pages 457–464, 2013. 1, 2, 3, 5, 6, 7

[9] E. Fuchs. Separating the fluorescence and reflectance components of coral spectra. *Applied Optics*, 40(21):3614–3621, 2001. 1, 2

[10] S. Han, Y. Matsushita, I. Sato, T. Okabe, and Y. Sato. Camera spectral sensitivity estimation from a single image under unknown illumination by using fluorescence. *IEEE Conference on Computer Vision and Pattern Recognition*, pages 805–812, 2012. 2

[11] S. Han, I. Sato, T. Okabe, and Y. Sato. Fast spectral reflectance recovery using dlp projector. *Asian Conference on Computer Vision*, pages 323–335, 2010. 1

[12] M. Hullin, M. Fuchs, I. Ihrke, H.-P. Seidel, and H. Lensch. Fluorescent immersion range scanning. *ACM Trans. Graph.*, 27(3):87:1–10, 2008. 2

[13] G. Johnson and M. Fairchild. Full-spectral color calculations in realistic image synthesis. *IEEE Computer Graphics and Applications*, 19(4):47–53, 1999. 1, 2

[14] S. Kim, S. Zhuo, F. Deng, C. Fu, and M. Brown. Interactive visualization of hyperspectral images of historical documents. *IEEE Trans. Visualization and Computer Graphics*, 16(6):1441–1448, 2010. 1

[15] A. Lam and I. Sato. Spectral modeling and relighting of reflective-fluorescent scenes. *IEEE Conference on Computer Vision and Pattern Recognition*, pages 1452–1459, 2013. 1, 2, 3

[16] J. Leland, N. Johnson, and A. Arecchi. Principles of bispectral fluorescence colorimetry. *Proc. SPIE*, 3140:76–87, 1997. 2

[17] L. Maloney. Evaluation of linear models of surface spectral reflectance with small numbers of parameters. *J. Opt. Soc. Am. A*, 3(10):1673–1683, 1986. 3

[18] G. McNamara, A. Gupta, J. Reynaert, T. Coates, and C. Boswell. Spectral imaging microscopy web sites and data. *Cytometry Part A*, 69(8):863–871, 2006. 3, 6

[19] J. Park, M. Lee, M. Grossberg, and S. Nayar. Multispectral imaging using multiplexed illumination. *IEEE International Conference on Computer Vision*, pages 1–8, 2007. 1

[20] J. Parkkinen, J. Hallikainen, and T. Jaaskelainen. Characteristic spectra of munsell colors. *J. Opt. Soc. Am. A*, 6(2):318–322, 1989. 3

[21] I. Sato, T. Okabe, and Y. Sato. Bispectral photometric stereo based on fluorescence. *IEEE Conference on Computer Vision and Pattern Recognition*, pages 270–277, 2012. 2

[22] J. Suo, L. Bian, F. Chen, and Q. Dai. Bispectral coding: compressive and high-quality acquisition of fluorescence and reflectance. *Optics Express*, 22(2):1697–1712, 2014. 1, 2

[23] S. Tominaga, T. Horiuchi, and T. Kamiyama. Spectral estimation of fluorescent objects using visible lights and an imaging device. *Proc. of the Color and Imaging Conference*, pages 352–356, 2011. 1, 2

[24] T. Treibitz, Z. Murez, B. Mitchell, and D. Kriegman. Shape from fluorescence. *European Conference on Computer Vision*, pages 292–306, 2012. 2

[25] C. Zhang and I. Sato. Separating reflective and fluorescent components of an image. *IEEE Conference on Computer Vision and Pattern Recognition*, pages 185–192, 2011. 2, 3

[26] Y. Zheng, I. Sato, and Y. Sato. Spectra estimation of fluorescent and reflective scenes by using ordinary illuminants. *European Conference on Computer Vision*, pages 188–202, 2014. 1, 3